NMR characterization of proton exchange membranes in controlled hygrometry conditions

Christine Mrad, Jean-Christophe Perrin, Assma El Kaddouri, Laouès Guendouz, Kévin Mozet, Jérôme Dillet, Olivier Lottin

NMR characterization of proton exchange membranes in controlled hygrometry conditions

Christine Mrad[a], Jean-Christophe Perrin[a,*], Assma El Kaddouri[a], Laouès Guendouz[a], Kévin Mozet[a], Jérôme Dillet[a], Olivier Lottin[a]

[a] *Université de Lorraine, CNRS, LEMTA, F-54000 Nancy, France*

* *corresponding author*

Email addresses: christine.mrad@univ-lorraine.fr (C. Mrad), jean-christophe.perrin@univ-lorraine.fr (J.-C. Perrin), assma.el-kaddouri@univ-lorraine.fr (A. El Kaddouri), laoues.guendouz@univ-lorraine.fr (L. Guendouz), kevin.mozet@univ-lorraine.fr (K. Mozet), jerome.dillet@univ-lorraine.fr (J. Dillet), olivier.lottin@univ-lorraine.fr (O. Lottin).

Abstract

NMR methods are highly sensitive to the state of water adsorbed in ionomer membranes for PEM fuel cells and electrolyzers. This study demonstrates the potential of NMR and MRI to reliably and accurately determine a wide range of water parameters such as proton chemical shift, transverse relaxation time, water content, and membrane thickness. Measurements are carried out *in-situ* in membranes in contact with humid air flows that are precisely controlled in terms of flow rate, temperature, and humidity. This precise management of the climatic conditions makes it possible to detect very small variations in the parameters measured, linked to the hydrothermal history of the membrane described in the literature. This history is erased when the membrane is humidity cycled several times. In addition, we demonstrate the use of this MRI imaging method to determine the resistance to water transfer across the membrane/humid air interface under steady-

state conditions. Finally, we propose a refinement of the imaging method that reduces acquisition time by a factor of two, without degrading the 1D water content profile. This improvement gives us access to the study of transient hydration regimes typical of PEMFC and PEME operation.

Keywords: PEMFC, PEME, water transfer, NMR, MRI, water profile

1. Introduction

Hydrogen has a notable role to play in supporting announced government climate commitments and to enhance energy security. In 2021 the USA announced a climate goal of cutting emissions 50% below 2005 levels by 2030 while the European Commission proposed to cut greenhouse gas emissions by at least 55%, also by 2030 [1]. A large number of initiatives aim to advance programs and projects that accelerate the commercialization and deployment of hydrogen and fuel cell technologies across all areas of the economy. Ultimately, it seeks to ensure hydrogen's place as a key enabler in the global clean energy transition. Proton Exchange Membrane Fuel Cells (PEMFC) and Proton Exchange Membrane Electrolyzers (PEME) are important players in the hydrogen economy. These systems have now reached a good technological maturity and many commercial solutions are operational. Research & Development focuses mainly on reducing the costs (*e.g.* by reducing the amount of catalyst) and increasing the durability of the components (*e.g.* by limiting the ageing of the membrane/electrode (MEA) assembly) [2, 3]. However, more fundamental studies are still needed to better understand the limitations induced by the decrease in platinum content in MEAs, both in terms of operation and aging of the electrodes and the ionomer membrane. More specifically, a better understanding of the water transport across the membrane/electrode interface is still required. It is thus necessary to use methods that can probe the properties of water within the membrane. To this end a number of experimental approaches have long been developed and used to measure the water profile through the PEM membrane, either *in-situ,* when the membrane is subjected to controlled temperature and humidity conditions [4-7], or *in-operando*, when the membrane is in an operational PEMFC [8-11]. Review articles detail the approaches that have been most productive [12-14]. Among them, nuclear magnetic resonance (NMR) and magnetic resonance imaging (MRI) have been shown to be effective in

studying the distribution and properties of water in the membrane. MRI has been used in particular to measure 1D water profiles in the membrane thickness with a spatial resolution down to 6 µm per point and an acquisition time of a few minutes per profile. Depending on the protocol used, the measurements could be performed *in-situ* [7, 15, 16] or *in-operando* [17-19]. In some studies, dedicated methodologies had to be used in order to adapt the NMR hardware, *i.e.* the radio frequency (RF) coil, to the 2D geometry of the membrane. The objective was twofold: to increase the signal-to-noise ratio of the measurement by placing the RF coil ideally with respect to the plane of the membrane [20] and to allow the measurement even when the carbonated gas diffusion layer (GDL) is adjacent to the membrane and must therefore be traversed by the RF magnetic field produced by the coil [16]. The experimental developments also concerned the improvement of the measurement methods (the so-called "NMR sequences") in order to measure parameters that are directly related to the absolute water content of the membrane [15, 20]. In contrast, *in-situ* NMR studies have so far paid little attention to the precise control of air humidity conditions imposed on either side of the membrane. This is probably due to the difficulty of maintaining regulated relative humidity conditions inside the spectrometer. The properties of the membrane however are very sensitive to variations in water content and so are the NMR parameters that can be accessed experimentally [21].

MRI imaging of the hydration profile across the membrane under unsaturated air conditions, both in steady state and during transient regimes could provide a good deal of valuable information regarding both water transfer at the membrane/electrode interface and diffusion properties in the bulk of the membrane. In this paper we present a device and a methodology capable of finely measuring the NMR properties of water in proton exchange membranes under controlled hygrometric conditions. The method, demonstrated on a thick Nafion membrane, allows to

measure the NMR properties of the water protons adsorbed in the polymer and the 1D through-plane water content profile with a good spatial and temporal resolution. We also present a basic improvement of the measurement sequence in order to accelerate the acquisition and lower the experimental time to about 2 min 24 seconds / profile, sufficient to have access to the quantitative evolution of the water distribution during transient hydration or drying regimes.

2. Materials and methods

2.1. Experimental setup

2.1.1 ***Humid air generator***

The global layout of the experimental setup is described in Figure 1. It mainly includes the measuring cell in which the studied membrane is placed, an air generator with controls relative humidity (RH), temperature and flow rate, and the NMR spectrometer.

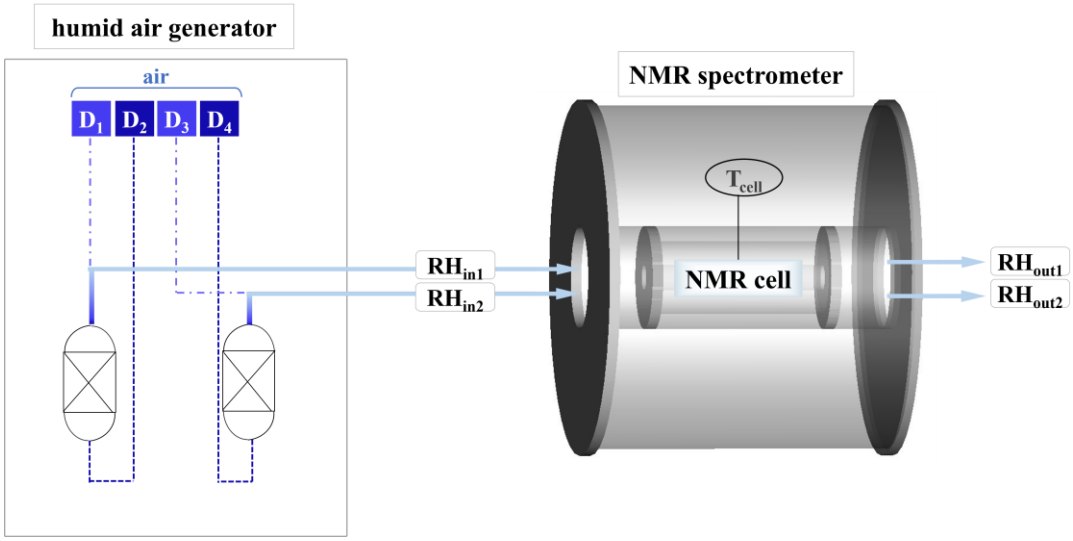

Figure 1. Schematics of the experimental setup.

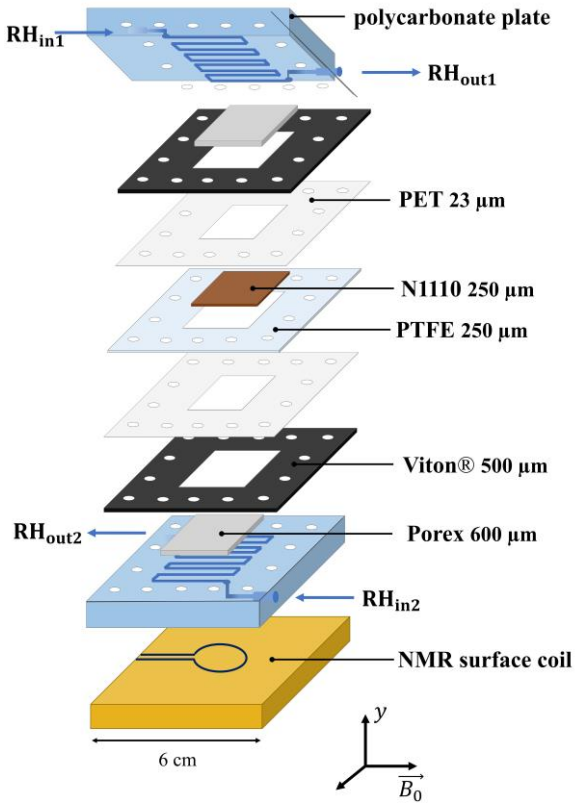

Figure 2. Detailed view of the different layers and materials of the NMR cell.

85

86 The humid air generator can produce two separated flows of humid air with flow rates in the range
87 $[0.05\text{–}1\ Nl/min]$, $RH = [0 - 95\ \%]$ and $T = [15 - 30°C]$. Each stream is generated by mixing
88 known volumes of dry and fully saturated air. The relative volumes are calculated based on the
89 desired flow rate and the temperature of the measuring cell, determined with a thermocouple
90 placed as closed as possible to the front of the NMR spectrometer. The relative humidity of the
91 streams at the inlet (RH_{in1}, RH_{in2}) and outlet (RH_{out1}, RH_{out2}) of the cell are recorded using four
92 VAISALA HMP7 Relative Humidity and Temperature Probes. The probes are heated to prevent
93 water condensation and allow the measurement in a wide range of RH values, with an accuracy up
94 to $\pm 0.8\ \%\ RH$ (value given by the manufacturer [22]). As the stray field of the NMR spectrometer

propagates far from the magnet, the air generator should be placed at a distance of about $2-3\ m$ from it. The air inlet and outlet tubings are wrapped with heating cords and insulated with foam to avoid water condensation. The temperature of the cords is regulated at 65°C.

2.1.2 ***NMR cell***

The measuring cell (Figure 2) must be able to supply a membrane with humid air on both sides in a homogeneous way. The materials must also be compatible with the presence of strong magnetic fields and not interfere with the NMR measurement. The humid air is fed into polycarbonate (PC) plates with serpentine channels $1\ mm$ wide and $0.8\ mm$ deep. The two air streams flow in countercurrent. The membrane sample ($2.7 \times 2.7\ cm^2$) is placed in the center of a PTFE layer which thickness is approximately the same as the nominal thickness of the membrane ($250\ \mu m$) and between two $23\ \mu m$ thick polyethylene terephthalate (PET) layers to prevent air leakage. Gas diffusion layers (GDL) homogenize the distribution of air coming from the bipolar plates. They are composed of $600\ \mu m$ thick Porex® sheets ($2.7 \times 2.7\ cm^2$) placed in the center of $500\ \mu m$ Viton™ seals. Porex® is a polyethylene-based porous media used in filtration and ventilation applications. The pore size is in the range $40-100\ \mu m$. The whole cell is clamped with nylon screws on the plate on which is engraved the radio frequency surface coil used to perform the NMR measurement (see next paragraph).

2.2. NMR and MRI protocols

The NMR experiments are performed on a Bruker BioSpec 24/40 spectrometer operating at the proton Larmor frequency of $100.36\ MHz$. The system is equipped with a $6\ cm$ ID magnetic field gradient system (BGAs) producing a maximum intensity of $1\ T/m$. The NMR probe is a custom-built single turn $1\ mm$ wide copper strip loop printed on CuFlon® (Polyflon Company). The internal and external diameters are $1.8\ cm$ and $2.0\ cm$ respectively. This coil is used for both

radiofrequency emission and NMR signal reception. More details about its design are given in a previous publication [7]. This kind of two-dimensional probe is suitable for the characterization of thin films [23]. The sensitivity is best when the plane of the object (the membrane) is placed at a distance equal to half the coil radius. Since the thickness of the N1110 membrane is small compared to the coil radius, there is no need to apply a correction due to the negligible inhomogeneity of the RF field in the depth of the membrane.

The different layers of materials were chosen so that they did not produce an NMR signal (Viton, PTFE) or the produced signal was very different from that of the water signal in the membrane. This is the case for hydrocarbon plastics such as Porex®, PET and PC, which produce a solid-like proton NMR signal (with very short NMR relaxation times T_2) that contributes to the NMR spectrum only in the baseline. Note that this background signal also contains the contribution of all the plastics surrounding the RF coil (such as the PMMA frame that supports the RF coil plate). The proton spectra were obtained by performing the Fourier transform of the FID temporal signal obtained after the application of a 23 μs-long 90° RF pulse. The relaxation time T_2 was determined by fitting the time evolution of the spin-echo amplitude during a CPMG sequence [24] by a single exponential function. The echo time was $TE = 2\ ms$. The through-plane water profiles were measured using the 1D spin-echo single-point imaging sequence (SE-SPI) introduced by Ouriadov and coworkers for the NMR characterization of thin films, including a Nafion membrane [20]. The temporal sequence is depicted in Figure 3. The combination of the two RF pulses $90° - 180°$ at times $t = 0$ and $t = TE/2$ produces a spin echo signal which is recorded at time $t = TE$. The through-plane spatial coordinate y is encoded in a one-dimensional reciprocal space by the variable $k_y = \gamma . g_y . t_{enc}$, where γ is the proton gyromagnetic ratio, g_y is the amplitude of the magnetic field gradient and t_{enc} is the encoding time, *i.e.* the time during which the field gradient is turned

on. The acquisition of an NMR intensity profile containing N_p points consists in recording the spin echo intensity at $t = TE$ for each value of the magnetic field gradient in the interval $[-g_{max}; +g_{max}]$ divided into N_p values. The repetition time TR separating the acquisition of two consecutive points in the reciprocal space is parameterized by the longitudinal relaxation time T_1 and must verify $TR \sim [3 - 5] \times T_1$ to ensure the return to equilibrium of the nuclear magnetization between two experiments. The complex signal intensity is written:

$$S(k_y) = \int S(y)\, exp[i2\pi k_y . y]dy \qquad \text{Eq. 1}$$

where $S(y)$ is the spatial NMR intensity profile, determined from Fourier transformation. The intensity profile is related to the water concentration profile $\lambda(y)$ by:

$$S(y) = K.\lambda(y) exp\left[\frac{-TE}{T_2(\lambda)}\right]\left(1 - exp\left[\frac{-TR}{T_1(\lambda)}\right]\right) \qquad \text{Eq. 2}$$

where K is a constant and the relaxation times $T_1(\lambda)$ and $T_2(\lambda)$ are functions of the water content. When the repetition time TR is sufficiently large, the NMR intensity is only weighted by the transverse relaxation term:

$$S(y) = K'.\lambda(y) exp\left[\frac{-TE}{T_2(\lambda)}\right] \qquad \text{Eq. 3}$$

Under this condition, when the membrane is in thermodynamic equilibrium and is exposed to two humid air flows with the same relative humidity on both sides, the water content profile can be inferred from the intensity profile using a calibration procedure. The water sorption isotherm, measured at the same temperature using a dynamic vapor sorption analyzer (IGAsorp from Hiden Isochema, Warrington, England), provides the relationship between relative humidity and water content [The measurement is shown Figure SI1 of the Supplementary Information].

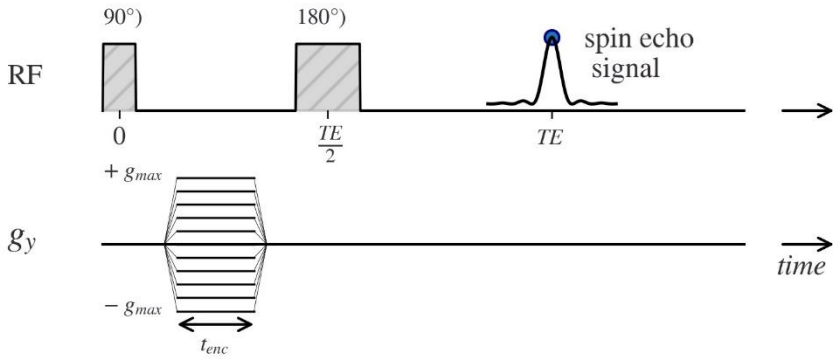

Figure 3. Timeline showing the main events that take place during the SE-SPI sequence.

159

160 The pixel size Δy is determined by the maximum amplitude of the field gradient g_{max} according
161 to:

$$\Delta y = \frac{\pi}{\gamma . g_{max} . t_{enc}} \qquad \text{Eq. 4}$$

162 The resolution limit (related to the minimum value of Δy) is therefore theoretically determined by
163 the maximum value of the field gradient that can be produced by the gradient coils. In reality, this
164 limit, extensively examined by Gravina and Cory [25], is limited by the mean square displacement
165 7of the water molecules during the echo time (TE), which is about $\Delta y_{min} = \sqrt{2 D_s TE} \cong 4\ \mu m$ for
166 $TE = 15\ ms$ and $D_s = 5.10^{-10} m^2/s$, the approximate value of the water self-diffusion
167 coefficient at $25°C$ in a water saturated Nafion membrane [21]. Unlike frequency encoding
168 methods, SPI techniques use a phase encoding scheme. This method is preferred for imaging water
169 in ionomer membranes because it is insensitive to imaging artifacts resulting from the dependence
170 of NMR chemical shift on membrane water content (as observed on Figure 7). In this study the
171 hydration profiles were measured using an encoding time $t_{enc} = 3\ ms$, a maximum gradient
172 strength $g_{max} = 0.375\ T/m$, 128 encoding steps, $TE = 7.5\ ms$ and $TR = 500\ ms$. The spatial

"resolution" is $\Delta y = 9.776\ \mu m/point$ and the field of view $FOV = 1.251\ mm$. Finally, it should be mentioned that the measurements of the hydration profiles are performed after carefully aligning the plane of the membrane orthogonal to the direction of the imaging gradient (y). The alignment procedure, described in reference [7], is critical in order to obtain profiles with square edges. The thickness of the membrane measured on the profiles is deduced from the variation of the NMR intensity when crossing the interface between the outside and the inside of the material. The inflection point is considered as the edge of the membrane and is obtained numerically by the determination of the maximum and minimum of the second derivative of the thickness with respect to the distance.

3. Results

3.1 Performance of the humid air generator

The performance of the humid air generator was evaluated under the same conditions as in the experiments that are described later (paragraph 3.2), i.e. with the same air flow rate ($30\ NL/h = 500\ mL/min$) and temperature ($T = 23.4 \pm 0.2°C$). The polymer membrane was replaced for the performance test by an impermeable PET layer so that the gas outlets were directly connected to the inlets and no water flow passed through the membrane plane. The air humidity was varied in the range $[10\% - 95\%]$ in 3 hours long step. Since the cell's clamping screws are made of nylon, the air tightness of the cell was checked by immersing it in water. The test was repeated several times and no air bubbles were observed. An example of the measurements is shown in Figure 4, where the relative humidity of two air streams, at the inlet and outlet of the cell, are plotted as a function of time. The accuracy of the relative humidity is shown in Figure 5(a), while the standard deviation is plotted in Figure 5(b).

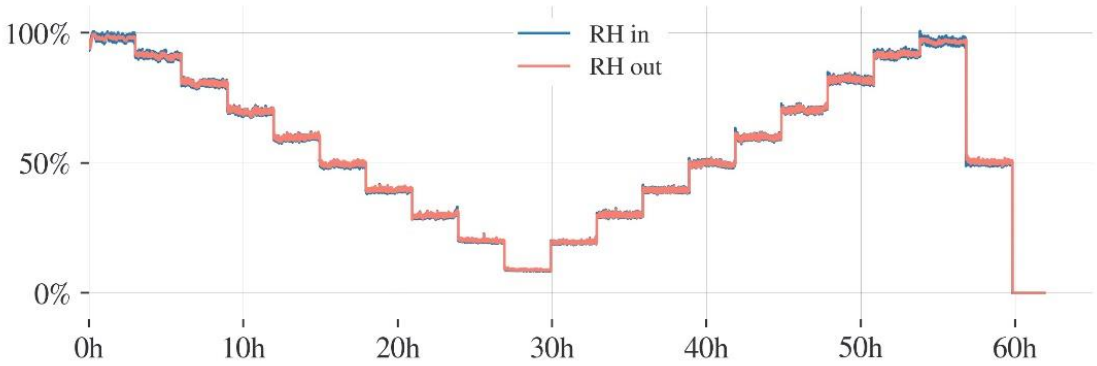

Figure 4. Performance test of the humid gas generator. Relative humidity of the cell inlet and outlet gases as a function of time.

195

196 The overall tests show that:

197 - The system is able to generate and maintain humid airflow over the entire relative humidity
198 range;
199 - Humidity stability is greater at low RH than at high RH;
200 - The measured values correspond to the setpoints with very good accuracy over the entire
201 range;
202 - The deviation relative to the setpoint ($\frac{RH_{\text{measured}} - RH_{\text{setpoint}}}{RH_{\text{setpoint}}} \times 100$) does not exceed 5%,
203 except when the humidity is very low, typically below 15% RH where it can reach 15%
204 at most ($15 \pm 2.25\ \%RH$).

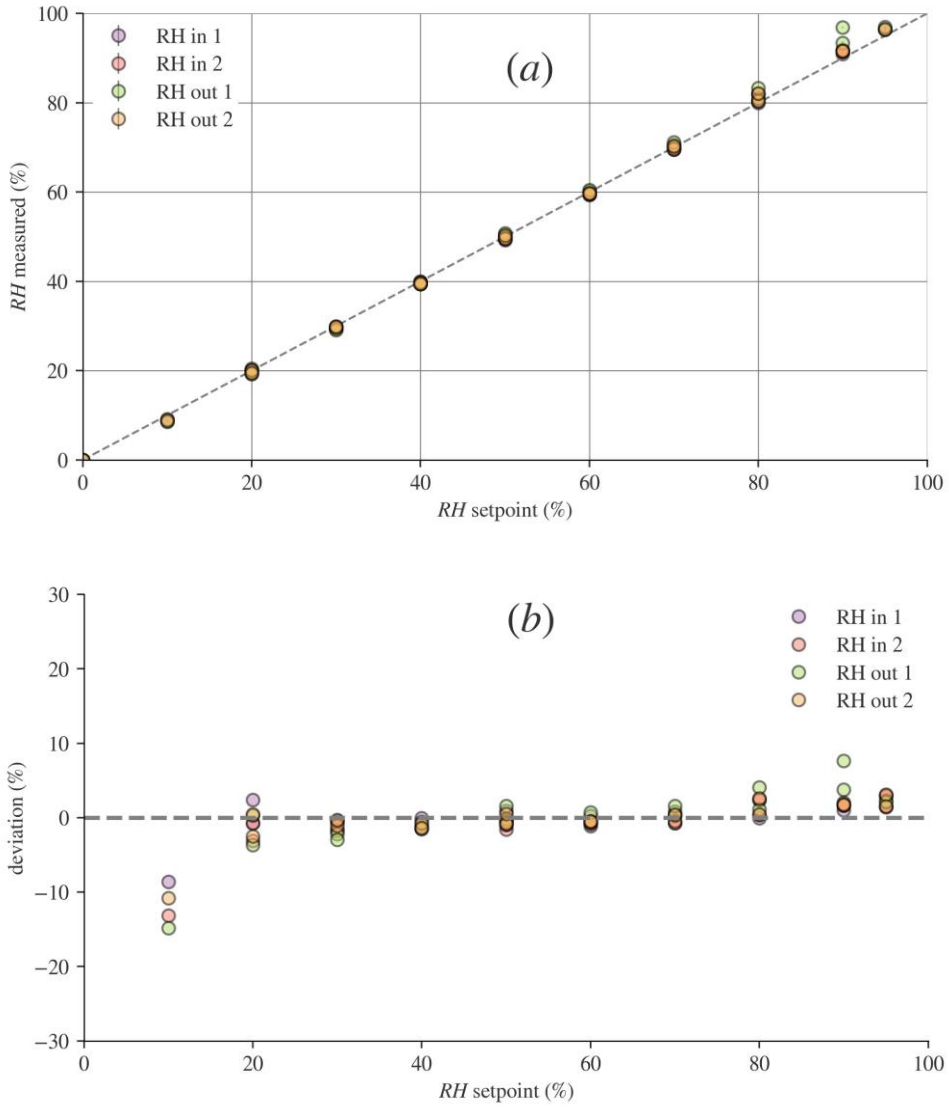

Figure 5. a) Accuracy of the humid air generator: RH measured as a function of the setpoint. b) Deviation in percent of the generated RH from the setpoint.

205

206 *3.2 In-situ NMR measurements of membrane properties*

207 The experiments discussed in this section were conducted by sending a stream of wet air
208 equilibrated at different relative humidity into the measuring cell containing the membrane sample.
209 The whole range of humidity was tested, from 10% to 90% RH at a temperature of 24°C, with
210 steps lasting three hours each. Five humidity cycles, called in the following "step sequences", are

discussed. The temporal variation of the step sequences is described in Figure 6. The total duration of the experiments was 108 hours. Each side of the membrane was exposed to an identical gas flow rate and relative humidity condition throughout all the described experiments. The NMR spectrum, T_2 transverse NMR relaxation time and water content profile were measured five times at each step. At the end of the steps, all the NMR parameters are stabilized which allows to consider that the membrane has reached a state of equilibrium with the humid air.

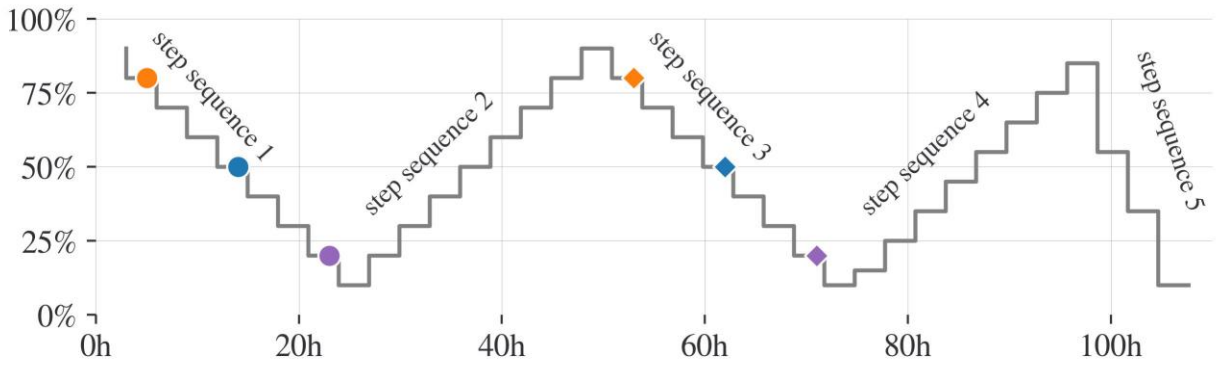

Figure 6. Temporal evolution of the air relative humidity (RH) during the five step sequences.

The proton NMR spectra measured during step sequence 2 are shown in Figure 7. They are composed of a single resonance line, as described in the literature [26, 27]. The different populations of protons are in a fast exchange regime relative to the time scale of NMR measurement which makes them indistinguishable [28]. The resonance line is centered at about 12 ppm in the driest membrane and shifts to low chemical shifts as the amount of water increases. This shift reflects the loss of confinement of water molecules and the dilution of the charges as water content increases. The evolution as a function of hydration is fast at low water content λ and moderate after [29], so that the evolution is ~ linear for $RH > 10\%$ (this can be seen later in the

document on Figure 10(a)). The bump observed on the right side of the spectra is a "solid" NMR signal produced by all proton-containing layers in the cell (PET, PC, Viton).

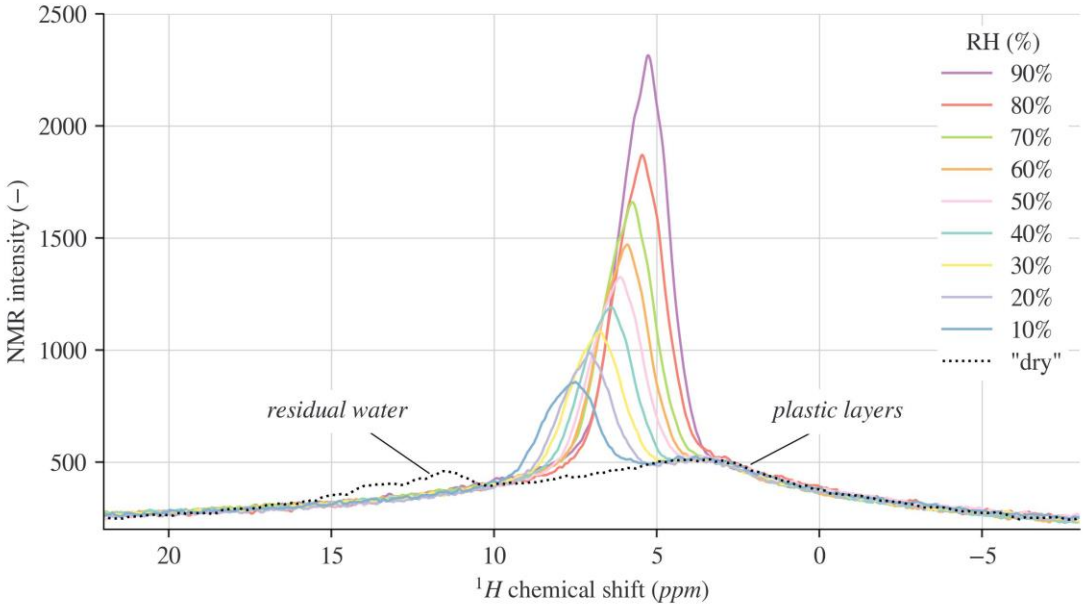

Figure 7. Evolution of the proton NMR spectrum as a function of equilibrium RH. The data were collected during step sequence 2 at the end of each humidity step.

The “dry” membrane was exposed to a flow of dry air for three hours. Therefore, the residual hydration is close to one molecule of water per ionic SO_3H site (three protons) [21, 28, 30]. As the chemical shift strongly depends on the water content, its determination can be seen as a good method to evaluate λ in a reliable and fast way. As the spectral resolution of the measurement is very high ($0.003\,ppm = 0.3\,Hz$ in the case of our measurements), the accuracy of the measurement can in theory be very good if accurate calibration is available. The perfluorosulfonic acid (PFSA) ionomer membranes have quite remarkable behaviors and are extremely sensitive to the thermal and hydric history. In particular, many studies demonstrate the influence of hydrothermal conditions on the mechanical, sorption and diffusion properties of water [31, 32].

The evaluation of the chemical shift is therefore a good way to characterize the effect of these environmental conditions. The chemical shift, the T_2 relaxation time and the 1D water content profile were systematically measured during the five different step sequences (Figure 8). The zoom on the right part of the figure corresponds to the evolution of each of the parameters during the first step sequence between $10\ h$ and $20\ h$. The NMR intensity and the thickness of the membrane are clearly stabilized at the end of each humidity step (note that if the error on the thickness is evaluated at $\pm$ 1 point then it is quite important ($\pm \sim 10\ \mu m$) relatively to the thickness variation between two steps). The chemical shift and the relaxation time have slightly less stabilized values at the end of the humidity steps. The chemical shift, as we have seen, has an excellent sensitivity and its determination is very accurate, while the determination of the transverse relaxation time relies on an exponential function fitting, which is less reliable and leads to less accuracy.

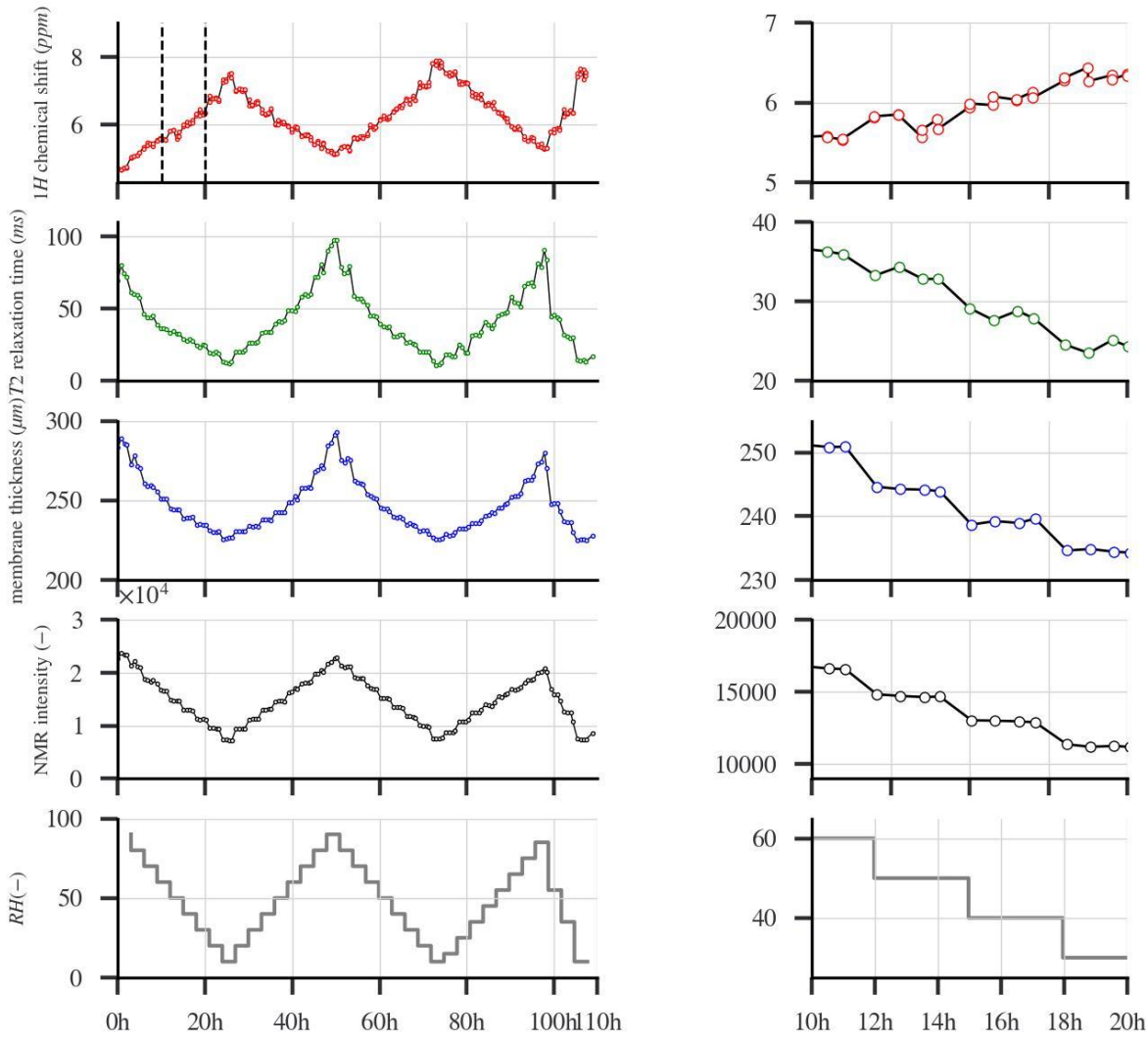

Figure 8. Evolution of ^{1}H chemical shift, T_2 relaxation time, NMR intensity and membrane thickness as a function of time during the five step-sequences. The experiments are repeated four to five times at each RH step. The right column shows a zoom in the period $10-20h$ during the first step-sequence.

249

250 Figure 9 shows the proton NMR spectra collected at the same RH values (20%, 50% and 80%)
251 during step sequence 1 and 3 (the times at which the measurements were performed are shown on
252 the timeline of Figure 6 using the same color codes). It can be seen that the resonance line
253 systematically shifts towards the high chemical shifts during the second dehydration sequence.
254 The initial state of the membrane at the beginning of sequence 1 corresponds to a fully hydrated

state, i.e. the sample has been soaked in water before being installed in the NMR cell. Water adsorption in liquid phase is known to induce a strong swelling of the membrane and to modify its mechanical properties: the swollen structure is softer and the water is very mobile. After a humidity cycle, the state of the water is different for the same RH values: after passing through a low humidity hydration stage, the polymer membrane is more rigid, the sorption capacity is slightly reduced and the water is less mobile at a given relative humidity. The effect of the hydration history of the membrane is therefore precisely detectable by measuring the NMR spectrum of water protons.

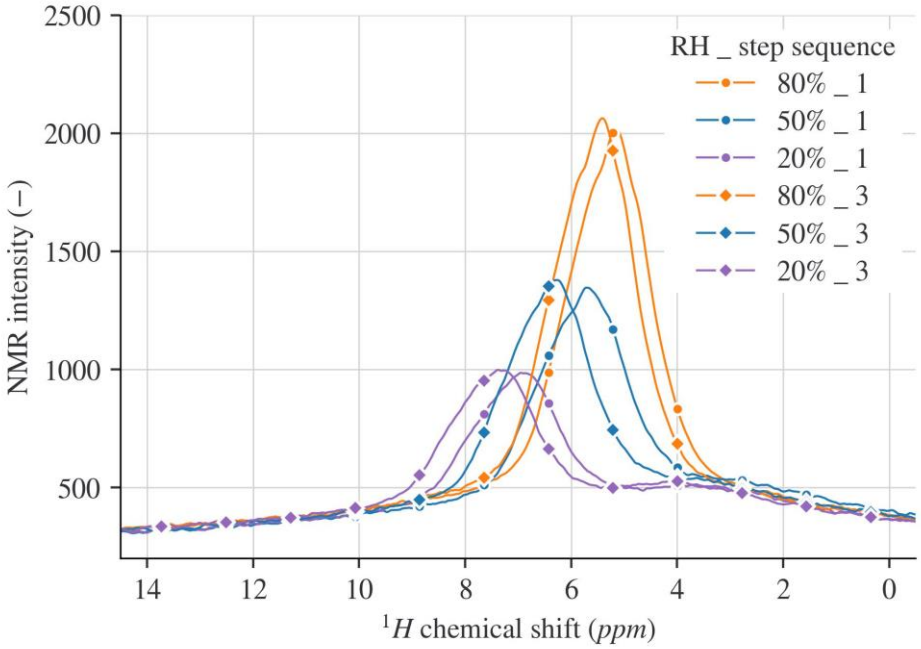

Figure 9. Comparison of NMR spectra measured at the same RH values during different step-sequences.

As the relative humidity of the air in contact with the membrane is further cycled, the chemical shift reaches a stable value, as shown in Figure 10(a) where this parameter is plotted for all step-sequence. The same observation can be deduced from the evolution of the transverse relaxation

time T_2 for the different step sequences (Figure 10(b)). The T_2 time, which also depends strongly on the membrane water content (the variation is almost an order of magnitude), varies by about 25% at $RH = 90\%$ between the first and the second step sequence. The effect is more visible for higher relative humidities, but in all cases the parameter reaches a plateau value when the gas humidity has been cycled several times. The NMR relaxation times T_1 and T_2 are markers of the water molecular dynamics in the membrane and are known to be dependent on temperature and hydration [33, 34]. The absolute value of the relaxation times is much lower than that measured on free water because of the confinement effects of water interacting with the internal surfaces of the pores in the microstructure of the membrane [35]. Paramagnetic interactions can also contribute strongly to the relaxation of the proton nuclear magnetization in samples containing impurities of metal cations such as sodium, copper or manganese [33, 36] which is frequently the case for membranes that have not undergone a specific washing protocol. The balance between the two effects is difficult to evaluate and the increase or decrease of T_2 values with water content can be observed in some cases due to subtle dilution effects during sorption that can lead to a change in the nature of the driving interaction between nuclear spins [37]. In the present study, the short T_2 times and their increase during humidity cycles in parallel with a decrease in the amount of water (Figure 10(c)) tend to prove that paramagnetic impurities are present in the membrane samples and are responsible for most of the nuclear relaxation. Regardless of the precise origin of the relaxation, T_2 reaches a plateau value at the end of the cycles, which corroborates the observations made on the chemical shift, and demonstrates a stabilization of the microstructure and mechanical properties of the membrane.

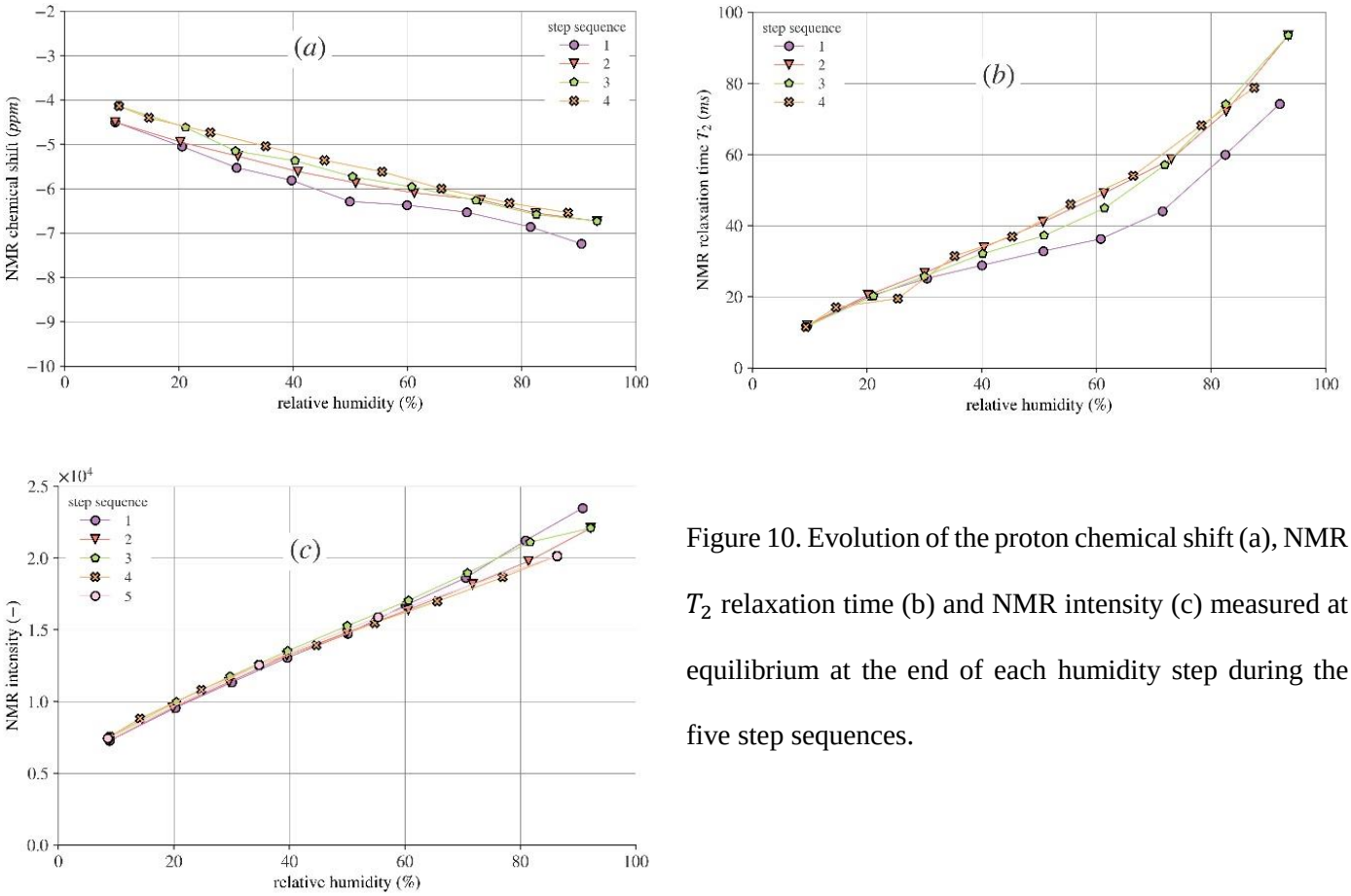

Figure 10. Evolution of the proton chemical shift (a), NMR T_2 relaxation time (b) and NMR intensity (c) measured at equilibrium at the end of each humidity step during the five step sequences.

The through-plane water content profiles measured at equilibrium during step sequence 3 are shown in Figure 11(a). The profiles are logically square because the moisture content of the air in contact with the membrane is the same on each side. Despite the rigorous alignment procedure, the edges are not very steep, the transition from the outside to the inside of the membrane being about four points wide. The main reason for this is the lack of flatness of the membrane on the detection surface of the NMR probe ($\sim 4\ cm^2$). Another reason is a possible variation in the chemical composition of the membrane at the interface. It is indeed known that the sulfonated sites of Nafion are less concentrated there [38]: the water content of the membrane would then be less important over a short distance near the interface. This effect, even if it is

supposed to be measurable, should not propagate over a large distance: less than a few microns in any case. The water content (λ) plotted on the profiles was obtained from a calibration of the NMR intensity measured in the membrane at equilibrium with humid air (see Eq3) and the Nafion N1110 sorption isotherm (Figure SI1). The calibration curve is shown in Figure SI2 of the Supplementary materials. The variation in membrane thickness extracted from the profiles is shown in Figure 11(b). Like the NMR intensity, the shape of the curves is analogous to that of the sorption curve, with the thickness of the membrane varying approximately linearly with its water content (isotropic swelling). The error in thickness determination (at most +/- 1 point) is significant, so the difference between the curves for the different step sequences is less marked than it is in the case of NMR intensity (Figure 10(c)).

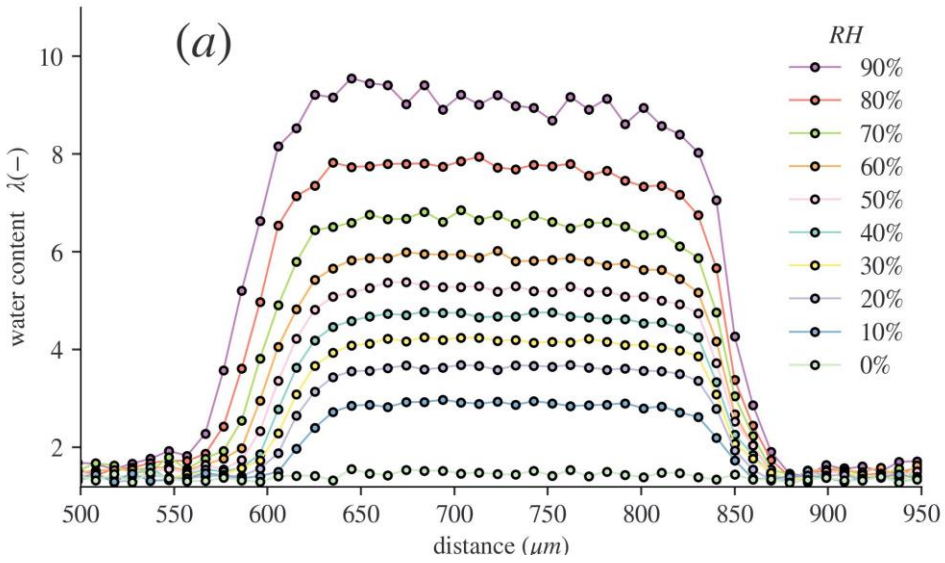

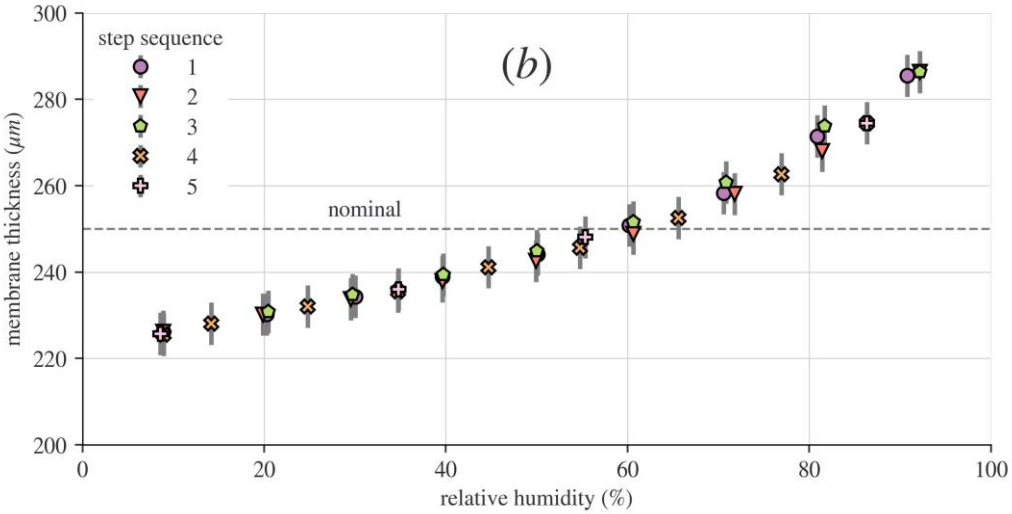

Figure 11. (a): through-plane water profiles in N1110 membranes at equilibrium with two streams of RH-controlled humid air. (b): Evolution of the membrane thickness as a function of relative humidity for the different step sequences. The nominal thickness of the membrane ($250\ \mu m$) is indicated with a dashed line.

3.3 Reduce acquisition time with partial acquisition

The motivation for using partial Fourier image reconstruction is the possibility of completing acquisition in roughly half the time of a normal profile. We used the most basic partial acquisition scheme which consists in acquiring only some of the 128 phase-encode steps without sacrificing spatial resolution. We tested different options (25% acceleration, 30% acceleration, etc..) and we finally chose to acquire only half of the points (50% acceleration) by removing the first 40 gradient steps (32%) and the last 24 (18%). An example of this procedure is shown Figure 12.

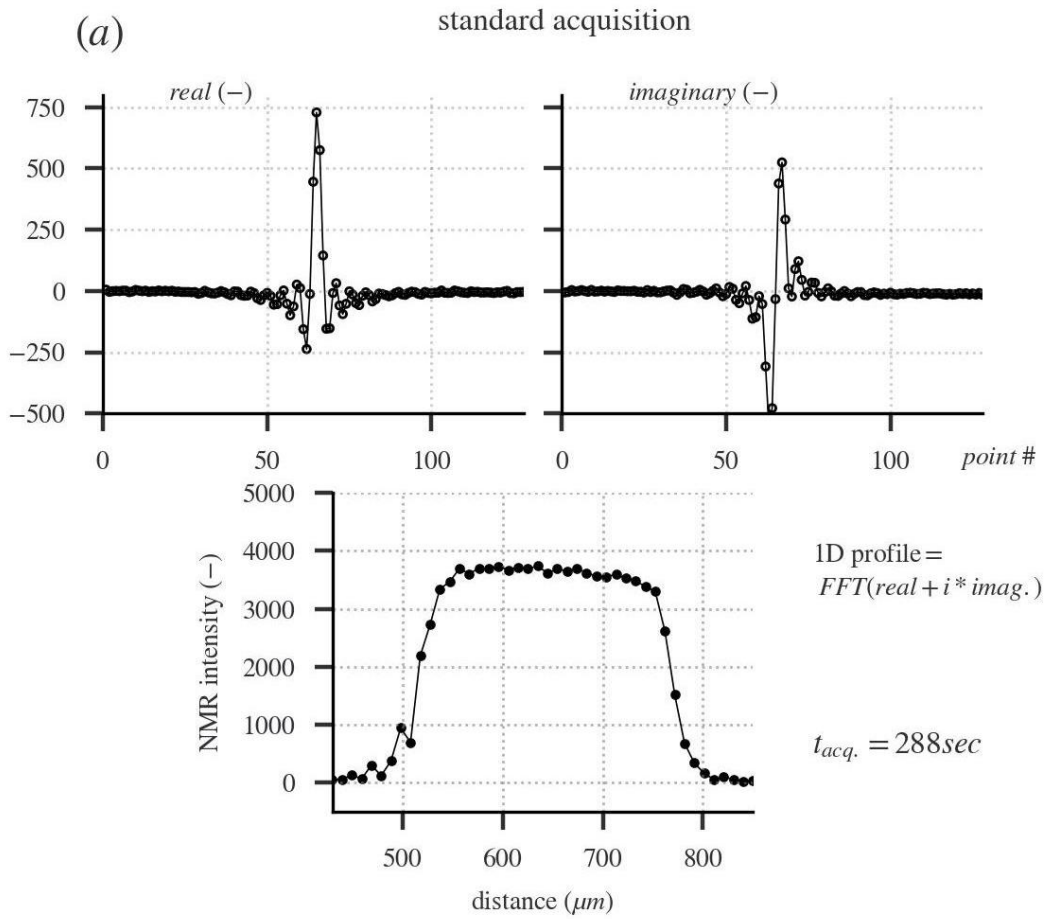
(a)
standard acquisition
real (−)
imaginary (−)
750
500
250
0
−250
−500
0
50
100
point #
NMR intensity (−)
5000
4000
3000
2000
1000
0
500
600
700
800
distance (μm)
1D profile =
FFT(real + i * imag.)
$t_{acq.} = 288sec$

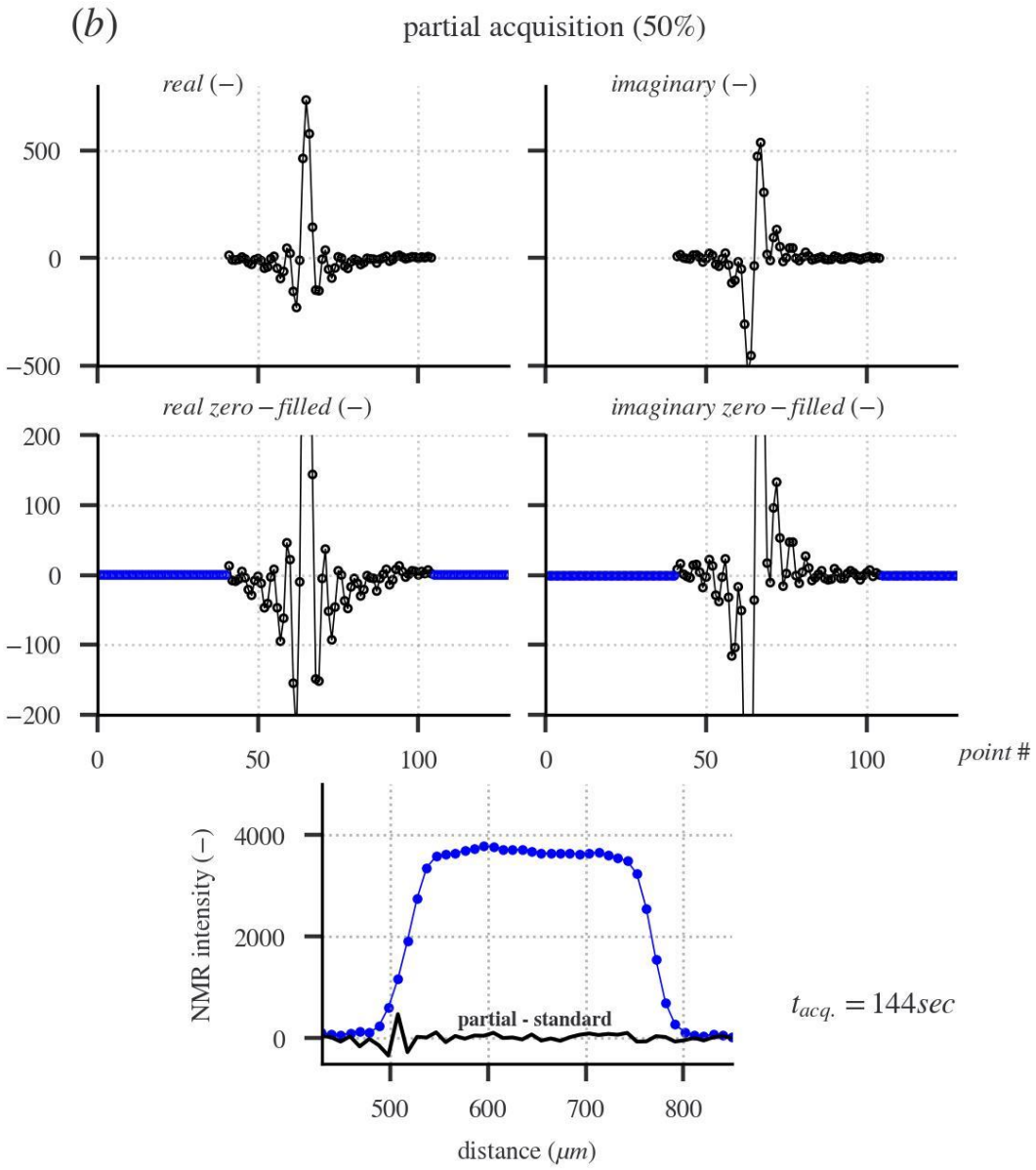

Figure 12. (a) Real and imaginary parts of the NMR signal during standard measurement of the water profile in the membranes. The profile is obtained by fast Fourier transform of these signals. (b) Partial acquisition performed on the same membrane a few moments after the first measurement. The first 40 points and the last 24 points were not recorded. Acquisition time is reduced by 50%. The data were then zero-filled (zoom and blue dots) before Fourier transformation to obtain the water profile.

316

Figure 12(a) shows the "standard" measurement (duration: 288 seconds), during which all 128 points are acquired. The 1D membrane hydration profile is obtained by Fast Fourier Transform from the real and imaginary NMR signals. It can be clearly seen that the majority of the signals are located in the center, and that the edges contain little information. After the partial acquisition of the experiment in Figure 12(b) (duration: 144 seconds) the 1D Fourier space was zero-filled during postprocessing. The quality of resulting profile obtained after Fourier transform is not deteriorated and is almost indistinguishable from the reference profile. The difference profile between the results of the two acquisitions shows just a small discrepancy near the left interface of the membrane where the reference profile shows an artifact. It is obvious that the partial acquisition strategy falls down when the 50% acceleration is concentrated on the first (or last) 64 points because in this case the most important part of the information, concentrated in the center of the Fourier line, is not acquired. The resulting profile is then largely distorted (Figure SI3 of the Supplementary Information).

4. Perspectives: record transient hydration profiles, study interfacial water transfer and determine the evolution of the diffusion coefficient

By using the partial acquisition approach, it is possible to make the acquisition time of the water profiles compatible with a time-resolved study of the water transfers that take place during transient regimes when the humidity of the air in contact with the membrane varies from one value to another. Results of such an experiment are presented on Figure 13. In this experiment, the membrane is initially at equilibrium with two streams of humid air at 80% RH. The air humidity is then suddenly switched from 80% to 0% on one side of the sample. The water content profiles and the water flux through the membrane are recorded as a function of time (Figure 13(b)). A steady state is reached after $\sim 2500s$ when the water profile and flux have stabilized. Then, the

air humidity is switched from 80% to 0% on the second side of the membrane and the profiles are observed for another $\sim 3000s$ period of time.

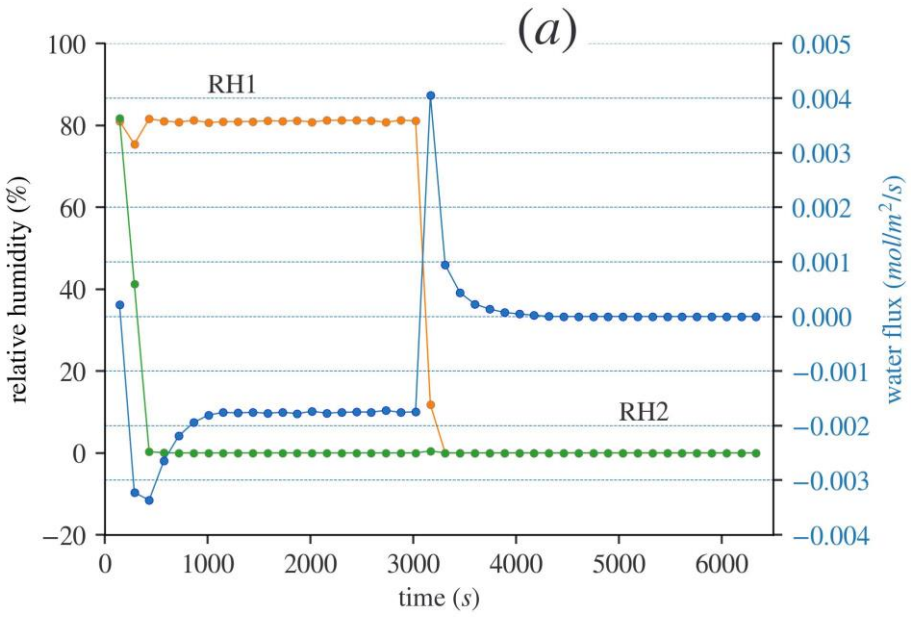

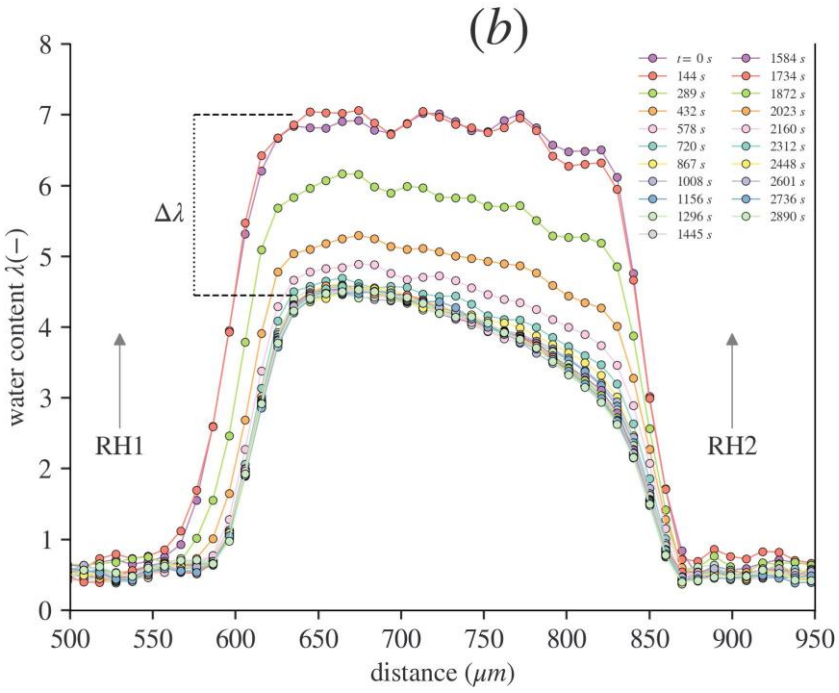

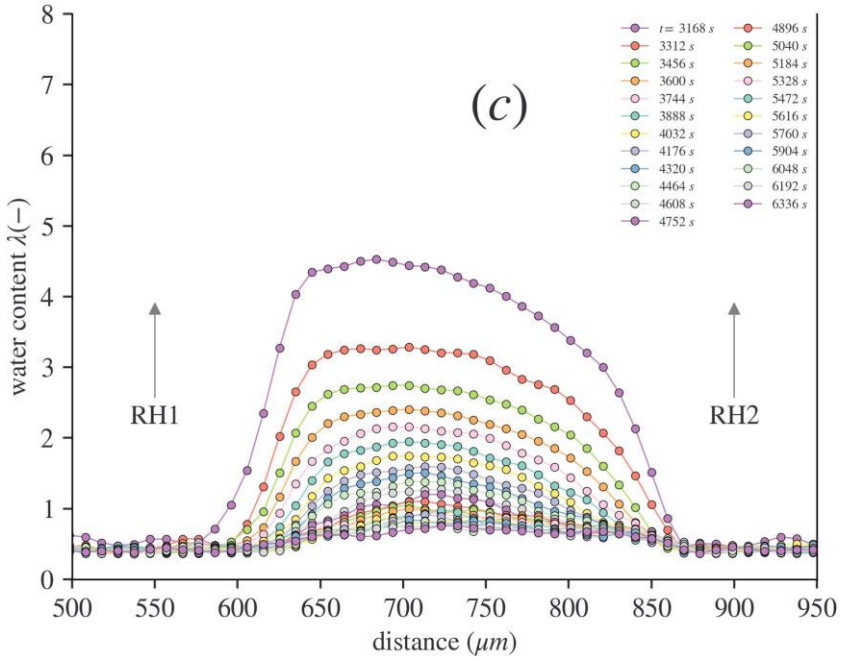

Figure 13. Time-resolved experiment. (a) Time variation of air relative humidity in contact with both sides of the membrane. In blue color (second axis): evolution of the water flux through the membrane. (b) Water profiles measured as a function of time following the initial switch of air humidity on one side of the sample (RH2) from 80% to 0%. (c) Water profiles measured as a function of time after switching the air humidity on the second side of the sample (RH1) from 80% to 0%.

342

343 During transient regimes water redistribution in the membrane is limited by the transport of water
344 across the membrane/vapor interface. In the literature, the interfacial resistance to water transport
345 across Nafion membranes has been characterized using water permeation measurements [36, 39,
346 40] and the results demonstrated that there is a competition between interfacial water transport and
347 water diffusion in the bulk of the membrane. Both effects depend on water content, and the
348 resistance due to diffusion scales linearly with the membrane thickness so that permeation
349 experiments have to be repeated multiple times by varying membrane thicknesses. This approach
350 is time-consuming. The method discussed here measures the water content of the membrane at the

membrane/vapor phase interfaces by means of MRI and the water flux through the membrane by means of the four RH probes. At steady state the interfacial resistance R_{int} can be evaluated using the following relationship between the driving force $\Delta\lambda$ (the difference between the water content at the interface and the water content at equilibrium, see Figure 13(b)) and the water flux φ :

$$R_{int} = C_{SO3H}\frac{\Delta\lambda}{\varphi} \qquad \text{Eq. 5}$$

where C_{SO3H} is the concentration in sulfonate ions in the membrane in mole/m^3 [41].

The water profile and the flux measured at $t = 2890\ s$ enable us to estimate an interface resistance approximately equal to $2.6.10^6\ m/s$, in full agreement with literature data [36, 38, 39, 41]. Using this procedure, it is possible to determine the evolution of interface resistance as a function of the air humidity to which the membrane is exposed.

Furthermore, as the measured steady states water profiles are not linear, the water diffusion coefficient is consequently a function of the membrane water content. The hydration dependence of the water diffusion coefficient in Nafion has been widely debated in the literature, and no clear consensus has yet emerged. As noted by Kosoglu and Weber, the difficulty comes from the nature of diffusion process in PFSA membranes, which is strongly dependent on the type of the measurement and the transport mechanisms it probes and become more complex over larger concentration gradients and time scales [38]. Using our experimental method and a suitable model of diffusive transport in the membrane, the shape of the water profiles and their evolution over time in response to changes in air humidity can be used to determine this concentration dependence. All these prospects are currently under study in our laboratory.

Conclusion

The important physicochemical parameters of PFSA membranes used in fuel cells and electrolyzers are highly dependent on the state of the water in the polymer: the water content, its dynamics, its interactions with the pores in the microstructure. Nuclear magnetic resonance is a proton-selective method that is extremely sensitive to the state of water in such complex structures. The method discussed in this study enables precise *in-situ* measurement of NMR parameters such as the proton chemical shift and the transverse relaxation times in a reliable and reproducible way in a membrane exposed to well controlled climatic conditions. This control allows us to detect very small variations in the water state linked to the hygrothermal history of the membrane. Measurements show that this history is erased by repeated cycling of air humidity in contact with the membrane. 1D MRI measurements through the membrane allow us to follow the evolution of the material's thickness, and precise calibration allows us to quantitatively determine the hydration profile in terms of the hydration number λ. Finally, a simple-to-implement partial acquisition refinement substantially reduces 1D image acquisition time without sacrificing quality. This opens the door to faster measurements that can be used to study transient phenomena at the membrane/moist air interfaces, when gas humidity setpoints vary at the edges of the membrane. All the prospects opened up by this study are potentially applicable to fuel cell and electrolyzer applications.

Funding

This research has received funding from the European Union's EIT Raw Materials project nº 19247 ALPE: "Advanced Low-Platinum hierarchical Electrocatalysts for low-T fuel cells".

References

[1] "https://climate.ec.europa.eu/eu-action/european-green-deal_en," ed.

[2] I. Fouzai, S. Gentil, V. C. Bassetto, W. O. Silva, R. Maher, and H. H. Girault, "Catalytic layer-membrane electrode assembly methods for optimum triple phase boundaries and fuel cell performances," *Journal of Materials Chemistry A*, vol. 9, no. 18, pp. 11096-11123, May 2021, doi: 10.1039/d0ta07470e.

[3] T. K. Maiti *et al.*, "Advances in perfluorosulfonic acid-based proton exchange membranes for fuel cell applications: A review," *Chemical Engineering Journal Advances*, vol. 12, p. 100372, 2022, doi: 10.1016/j.ceja.2022.100372.

[4] S. Deabate *et al.*, "Raman Microspectroscopy as a Useful Tool for In Situ and Operando Studies of Water Transport in Perfluorosulfonic Membranes for PEMFCs," *Fuel Cells*, vol. 14, no. 5, pp. 677-693, Oct 2014, doi: 10.1002/fuce.201300236.

[5] P. Huguet, A. Morin, G. Gebel, S. Deabate, A. K. Sutor, and Z. Peng, "In situ analysis of water management in operating fuel cells by confocal Raman spectroscopy," *Electrochemistry Communications*, vol. 13, no. 5, pp. 418-422, May 2011, doi: 10.1016/j.elecom.2011.02.008.

[6] G. S. Hwang, D. Y. Parkinson, A. Kusoglu, A. A. MacDowell, and A. Z. Weber, "Understanding Water Uptake and Transport in Nafion Using X-ray Microtomography," *Acs Macro Letters*, vol. 2, no. 4, pp. 288-291, Apr 2013, doi: 10.1021/mz300651a.

[7] M. Klein, J. C. Perrin, S. Leclerc, L. Guendouz, J. Dillet, and O. Lottin, "Spatially and Temporally Resolved Measurement of Water Distribution in Nafion Using NMR Imaging," *ECS Transactions*, vol. 58, no. 1, pp. 283-289, 2013, doi: 10.1149/05801.0283ecst.

[8] F. Xu, O. Diat, G. Gebel, and A. Morin, "Determination of transverse water concentration profile through MEA in a fuel cell using neutron scattering," *Journal of the Electrochemical Society*, vol. 154, no. 12, pp. B1389-B1398, 2007, doi: 10.1149/1.2794287.

[9] M. A. Hickner *et al.*, "Real-time imaging of liquid water in an operating proton exchange membrane fuel cell," *Journal of the Electrochemical Society*, vol. 153, no. 5, pp. A902-A908, 2006, doi: 10.1149/1.2184893.

[10] R. Satija, D. L. Jacobson, M. Arif, and S. A. Werner, "In situ neutron imaging technique for evaluation of water management systems in operating PEM fuel cells," *Journal of Power Sources*, vol. 129, no. 2, pp. 238-245, Apr 2004, doi: 10.1016/j.jpowsour.2003.11.068.

[11] C. Hartnig, I. Manke, R. Kuhn, S. Kleinau, J. Goebbels, and J. Banhart, "High-resolution in-plane investigation of the water evolution and transport in PEM fuel cells," *Journal of Power Sources*, vol. 188, no. 2, pp. 468-474, Mar 2009, doi: 10.1016/j.jpowsour.2008.12.023.

[12] S. Deabate, G. Gebel, P. Huguet, A. Morin, and G. Pourcelly, "3 In situ and operando determination of the water content distribution in proton conducting membranes for fuel cells: a critical review," *Energy & Environmental Science*, vol. 5, no. 10, pp. 8824-8847, Oct 2012, doi: 10.1039/c2ee21834h.

[13] L. M. Yan, Y. D. Hu, X. M. Zhang, and B. H. Yue, "Applications of NMR Techniques in the Development and Operation of Proton Exchange Membrane Fuel Cells," *Annual*

Reports on Nmr Spectroscopy, Vol 88, vol. 88, pp. 149-213, 2016, doi: 10.1016/bs.arnmr.2015.11.003.

[14] Q. Meyer, Y. C. Zeng, and C. Zhao, "In Situ and Operando Characterization of Proton Exchange Membrane Fuel Cells," *Advanced Materials*, vol. 31, no. 40, Oct 2019, Art no. 1901900, doi: 10.1002/adma.201901900.

[15] Z. H. Zhang, K. Promislow, J. Martin, H. J. Wang, and B. J. Balcom, "Bi-modal water transport behavior across a simple Nafion membrane," *Journal of Power Sources*, vol. 196, no. 20, pp. 8525-8530, Oct 2011, doi: 10.1016/j.jpowsour.2011.06.046.

[16] Z. H. Zhang, A. E. Marble, R. P. MacGregor, J. Martin, H. J. Wang, and B. J. Balcom, "Zero-mode TEM parallel-plate resonator for high-resolution thin film magnetic resonance imaging," *Canadian Journal of Chemistry-Revue Canadienne De Chimie*, vol. 89, no. 7, pp. 745-753, Jul 2011, doi: 10.1139/v11-018.

[17] Z. H. Zhang *et al.*, "Spatial and temporal mapping of water content across Nafion membranes under wetting and drying conditions," *Journal of Magnetic Resonance*, vol. 194, no. 2, pp. 245-253, Oct 2008, doi: 10.1016/j.jmr.2008.07.011.

[18] S. Tsushima, K. Teranishi, and S. Hirai, "Magnetic resonance imaging of the water distribution within a polymer electrolyte membrane in fuel cells," *Electrochemical and Solid State Letters*, vol. 7, no. 9, pp. A269-A272, 2004, doi: 10.1149/1.1774971.

[19] S. Tsushima, K. Teranishi, K. Nishida, and S. Hirai, "Water content distribution in a polymer electrolyte membrane for advanced fuel cell system with liquid water supply," *Magnetic Resonance Imaging*, vol. 23, no. 2, pp. 255-258, Feb 2005, doi: 10.1016/j.mri.2004.11.059.

[20] A. V. Ouriadov, R. P. MacGregor, and B. J. Balcom, "Thin film MRI - high resolution depth imaging with a local surface coil and spin echo SPI," *Journal of Magnetic Resonance*, vol. 169, no. 1, pp. 174-186, Jul 2004, doi: 10.1016/j.jmr.2004.04.015.

[21] L. Maldonado, J. C. Perrin, J. Dillet, and O. Lottin, "Characterization of polymer electrolyte Nafion membranes: Influence of temperature, heat treatment and drying protocol on sorption and transport properties," *Journal of Membrane Science*, vol. 389, pp. 43-56, 2012, doi: 10.1016/j.memsci.2011.10.14.

[22] "https://www.vaisala.com/en," ed.

[23] J. C. Perrin, C. Waldner, J. Bossu, A. Chatterjee, and U. Hirn, "Real time monitoring of the through thickness moisture profile of thin sheets using NMR," *Chemical Engineering Science*, vol. 251, Apr 2022, Art no. 117464, doi: 10.1016/j.ces.2022.117464.

[24] H. Y. Carr and E. M. Purcell, "Effects of Diffusion on Free Precession in Nuclear Magnetic Resonance Experiments," *Phys. Rev.*, vol. 94, no. 3, pp. 630-638, 1954.

[25] S. Gravina and D. G. Cory, "SENSITIVITY AND RESOLUTION OF CONSTANT-TIME IMAGING," *Journal of Magnetic Resonance Series B*, vol. 104, no. 1, pp. 53-61, May 1994, doi: 10.1006/jmrb.1994.1052.

[26] M. Robert, A. El Kaddouri, J. C. Perrin, S. Leclerc, and O. Lottin, "Towards a NMR-Based Method for Characterizing the Degradation of Nafion XL Membranes for PEMFC," *Journal of the Electrochemical Society*, vol. 165, no. 6, pp. F3209-F3216, 2018, doi: 10.1149/2.0231806jes.

[27] A. Guillermo, G. Gebel, H. Mendil-Jakani, and E. Pinton, "NMR and Pulsed Field Gradient NMR Approach of Water Sorption Properties in Nafion at Low Temperature," *Journal of Physical Chemistry B*, vol. 113, no. 19, pp. 6710-6717, May 2009, doi: 10.1021/jp8110452.

[28] N. J. Bunce, S. J. Sondheimer, and C. A. Fyfe, "Proton NMR method for the quantitative determination of the water content of the polymeric perfluorosulfonic acid Nafion-H.," *Macromolecules*, vol. 19, no. 2, pp. 333-339, Feb 1986, doi: 10.1021/ma00156a015.
[29] S. Tsushima, K. Teranishi, and S. Hirai, "Water diffusion measurement in fuel-cell SPE membrane by NMR," *Energy*, vol. 30, no. 2-4, pp. 235-245, Feb-Mar 2005, doi: 10.1016/j.energy.2004.04.013.
[30] F. N. Xu, S. Leclerc, O. Lottin, and D. Canet, "Impact of chemical treatments on the behavior of water in Nafion (R) NRE-212 by H-1 NMR: Self-diffusion measurements and proton quantization," *Journal of Membrane Science*, vol. 371, no. 1-2, pp. 148-154, Apr 2011, doi: 10.1016/j.memsci.2011.01.038.
[31] F. M. Collette, C. Lorentz, G. Gebel, and F. Thominette, "Hygrothermal aging of Nafion (R)," *Journal of Membrane Science*, vol. 330, no. 1-2, pp. 21-29, Mar 2009, doi: 10.1016/j.memsci.2008.11.048.
[32] F. M. Collette, F. Thominette, H. Mendil-Jakani, and G. Gebel, "Structure and transport properties of solution-cast Nafion (R) membranes subjected to hygrothermal aging," *Journal of Membrane Science*, vol. 435, pp. 242-252, May 2013, doi: 10.1016/j.memsci.2013.02.002.
[33] B. MacMillan, A. R. Sharp, and R. L. Armstrong, "An nmr investigation of the dynamical characteristics of water absorbed in Nafion," *Polymer*, vol. 40, no. 10, pp. 2471-2480, May 1999, doi: 10.1016/s0032-3861(98)00484-4.
[34] B. MacMillan, A. R. Sharp, and R. L. Armstrong, "N.m.r. relaxation in Nafion - The low temperature regime," *Polymer*, vol. 40, no. 10, pp. 2481-2485, 1999.
[35] J. C. Perrin, S. Lyonnard, A. Guillermo, and P. Levitz, "Water dynamics in ionomer membranes by field-cycling NMR relaxometry," *Journal of Physical Chemistry B*, vol. 110, no. 11, pp. 5439-5444, Mar 2006, doi: 10.1021/jp057433e.
[36] Q. A. Zhao, P. Majsztrik, and J. Benziger, "Diffusion and Interfacial Transport of Water in Nafion," *Journal of Physical Chemistry B*, vol. 115, no. 12, pp. 2717-2727, Mar 2011, doi: 10.1021/jp1112125.
[37] J. C. Perrin, S. Lyonnard, A. Guillermo, and P. Levitz, "Water dynamics in lonomer membranes by field-cycling NMR relaxometry," *Fuel Cells*, vol. 6, no. 1, pp. 5-9, Feb 2006, doi: 10.1002/fuce.200500094.
[38] A. Kusoglu and A. Z. Weber, "New Insights into Perfluorinated Sulfonic-Acid lonomers," *Chemical Reviews*, vol. 117, no. 3, pp. 987-1104, 2017, doi: 10.1021/acs.chemrev.6b00159.
[39] P. W. Majsztrik, M. B. Satterfield, A. B. Bocarsly, and J. B. Benziger, "Water sorption, desorption and transport in Nafion membranes," *Journal of Membrane Science*, vol. 301, no. 1-2, pp. 93-106, Sep 2007, doi: 10.1016/j.memsci.2007.06.022.
[40] P. Majsztrik, A. Bocarsly, and J. Benziger, "Water Permeation through Nafion Membranes: The Role of Water Activity," *Journal of Physical Chemistry B*, vol. 112, no. 51, pp. 16280-16289, Dec 2008, doi: 10.1021/jp804197x.
[41] S. Didierjean *et al.*, "Theoretical evidence of the difference in kinetics of water sorption and desorption in Nafion (R) membrane and experimental validation," *Journal of Power Sources*, vol. 300, pp. 50-56, Dec 2015, doi: 10.1016/j.jpowsour.2015.09.053.